

Second wave COVID-19 pandemics in Europe: A Temporal Playbook

Giacomo Cacciapaglia* and Corentin Cot†

*Institut de Physique des deux Infinis de Lyon (IP2I), UMR5822, CNRS/IN2P3, F-69622, Villeurbanne, France and
University of Lyon, Université Claude Bernard Lyon 1, F-69001, Lyon, France*

Francesco Sannino‡

*CP3-Origins & the Danish Institute for Advanced Study. University of Southern Denmark. Campusvej 55,
DK-5230 Odense, Denmark;*

*Dipartimento di Fisica E. Pancini, Università di Napoli Federico II — INFN sezione di Napoli
Complesso Universitario di Monte S. Angelo Edificio 6, via Cintia, 80126 Napoli, Italy.*

A second wave pandemic constitutes an imminent threat to society, with a potentially immense toll in terms of human lives and a devastating economic impact. We employ the epidemic renormalisation group approach to pandemics, together with the first wave data for COVID-19, to efficiently simulate the dynamics of disease transmission and spreading across different European countries. The framework allows us to model, not only inter and extra European border control effects, but also the impact of social distancing for each country. We perform statistical analyses averaging on different level of human interaction across Europe and with the rest of the world. Our results are neatly summarised as an animation reporting the time evolution of the first and second waves of the European COVID-19 pandemic. Our temporal playbook of the second wave pandemic can be used by governments, financial markets, the industries and individual citizens, to efficiently time, prepare and implement local and global measures.

Pandemics are increasingly becoming a constant menace to the human race, with COVID-19 being the latest example. A second wave is creeping back in Europe and is poised to rage across the continent by fall 2020.

In this letter we provide a statistical analysis of the temporal evolution of the second wave of infected cases, with the impact for various European countries. To model the spreading, we employ the *epidemic Renormalisation Group* (eRG) framework, recently developed in [1, 2]. It can be mapped [2, 3] into a time-dependent compartmental model of the SIR type [4]. The Renormalisation Group approach [5, 6] has a long history in physics with impact from particle to condensed matter physics and beyond. Its application to epidemic dynamics is complementary to other approaches [7–17].

The eRG approach consists in a set of first order differential equations apt to describe the time-evolution of the infected cases in a specific isolated region. It has been extended in [2] to include interactions among multiple regions of the world, without the need for powerful numerical simulations. The set of equations [2] reads

$$\frac{d\alpha_i}{dt} = \gamma_i \alpha_i \left(1 - \frac{\alpha_i}{a_i}\right) + \sum_{j \neq i} \frac{k_{ij}}{n_{mi}} (e^{\alpha_j - \alpha_i} - 1), \quad (1)$$

where

$$\alpha_i(t) = \ln \mathcal{I}_i(t), \quad (2)$$

with $\mathcal{I}_i(t)$ being the total number of infected cases *per million* inhabitants for region i and \ln indicating its natural logarithm. These equations embody, within a small number of parameters, the pandemic spreading dynamics across coupled regions of the world via the temporal evolution of α_i , which resembles the energy dependence of the interaction coupling appearing in fundamental interactions of particle physics.

The first term of the right-hand side in (1) characterises the epidemic evolution within a given region of the world. The infection rate γ_i , measured in inverse weeks, is responsible for how quick the epidemic evolves in the i -th region. Besides depending on the intrinsic virulent character of the epidemic, the size of γ_i can be controlled via social-distancing measures, with a flatter epidemic curve associated to smaller γ_i . It is well understood [4] that epidemic diffusion curves generally lead to plateaus in the total number of infected cases at late times. This is encoded in the parameter a_i , equal to the natural logarithm (\ln) of the total number of infected cases (per million) at the end of the epidemic wave.

The second term of the right-hand side in (1), first introduced in [2], is a source-term that takes into account human interaction across different regions of the world. Here, n_{mi} is the population of region- i in millions and k_{ij} represents the number of reciprocal travellers per week from region i to region j and vice-versa in units of million people. For a single country, i.e. France, we illustrate diagrammatically the connections given by the k_{ij} couplings in Fig. 1. We also consider an extra-source of infection modelled as a new region that we call Region-X ($i = 0$). We can interpret this region in various ways: for instance, this may represent an inflow of infections coming from outside of the regions of the world included in

* cacciapaglia@ipnl.in2p3.fr

† cot@ipnl.in2p3.fr

‡ sannino@cp3.sdu.dk

the simulation or, alternatively, Region-X may represent the effect of local hotspots of infections. Of course, it could also be a combination of the two effects.

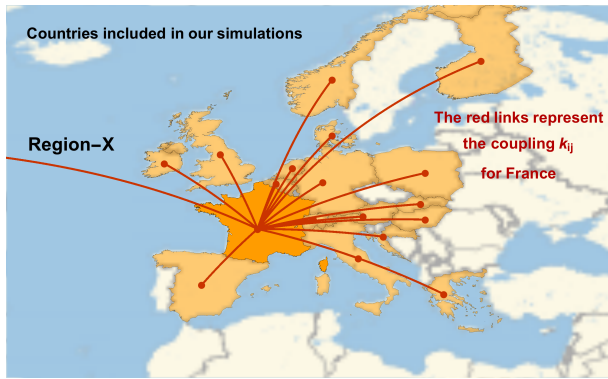


FIG. 1. Illustration of the connections k_{ij} between, i.e., France and the other countries considered in this study. Each line represents the exchange of infected cases. The line pointing outside the map represents the connection with Region-X, whose role is explained in the main text.

I. METHODOLOGY

To simulate the European second wave, we use as input parameters the values of γ_i and a_i stemming from the first wave. Predicting these parameters for the second wave is hard, as shown for instance in Ref. [18] via a *stochastic SEIR* model where very large fluctuations are found. This is one of the reasons why we choose for our simulations the parameters coming from the first wave. Additionally this choice has the advantage of endowing us with reasonable benchmark values. These parameters depend on social distancing measures enacted by each country during the first wave. The methodology of the fit for γ_i and a_i is described in [1, 2]. The values are reported in the first three columns of Table I at 90% confidence level. For the simulations we used the central values.

We now move to the interaction across the different European countries encoded in the matrix k_{ij} . We generate the entries of the matrix randomly with each value in the interval $10^{-3} - 10^{-2}$ and a flat probability. This translates in a range of 1k to 10k travellers per week across countries. In our earlier work [2] this interval was shown to be able to account for the peak delay in between countries.

As mentioned earlier, we also consider the extra-source of infection Region-X ($i = 0$) with a fixed number of infected cases. This region couples to the different European countries with randomly generated $k_{0i} = k_{i0}$ in the same range as above. To Region-X we can assign different interpretations. One could be that of an extra-European source (say the rest of the world) that still

couples to some or all European countries we consider. Another interpretation is that the coupling k_{0i} to Region-X represents an internal source of infection inside the i -th region. To provide a sensible value for the initial source, we considered the current number of total infected (5.2 millions) normalised to the world population in millions.

Specifically, we randomly generate 100 copies of the matrix k_{ij} to be used to repeat the simulation. The initial time of the second wave simulations is the calendar week 25, where we set the initial values for $\alpha_i = 0$ (while $\alpha_0 = \text{constant}$). We repeat the 100 simulations with the same set of k_{ij} for five cases, where we modify the coupling to Region-X as follows:

- We use the randomly generated $k_{0i} = k_{i0}$, in the range $10^{-2} - 10^{-3}$;
- We divide the k_{0i} by a factor of ten, implying a 90% reduction of the interaction with Region-X;
- We divide the k_{0i} by a factor of hundred, i.e. a 99% reduction;
- All the k_{0i} are set to zero except one, which we chose to be that of Spain;
- All the k_{0i} are set to zero except the ones for Croatia, Greece, Slovakia, Spain and Switzerland.

We consider the latter case e) as the most realistic, as the five chosen countries already show signs of a second wave as of calendar week 30. For each of these five cases, we average over the 100 simulated matrices k_{ij} to extract the location of the peak of the newly infected cases for the second wave per each country. The results are summarised in last five columns of Table I with the errors representing one standard deviation. The time is given in 2020 calendar weeks.

II. RESULTS

We first discuss the results for the simulations in case e), which are more realistic *vis à vis* the current situation in Europe, as of week 30. As a test, in Fig. 2 we show the outcome for Croatia, where we also include the first wave from the fit, compared to the actual data points (from [worldometers.info](https://www.worldometers.info)). The blue curve is the result of one of the 100 case e) simulations, while the orange curve contains the same simulation shifted back by three weeks. The shift could be achieved by increasing the coupling k_{i0} for Croatia by about one order of magnitude (i.e. of the order of 0.1), to reflect the presence of hotspots inside the country. This is already observable from the data starting at week 25. The figure clearly shows that the infection rate γ for the second wave is very close to that of the first wave and that the simulation provides a reasonable understanding of the second

First wave parameters			Second wave simulations: peak timing (calendar weeks 2020)				
	a	γ	case a	case b	case c	case d	case e
Austria	7.463 ± 0.007	0.99 ± 0.025	30.4 ± 0.5	32.4 ± 0.5	34.7 ± 0.6	38.4 ± 0.9	34.2 ± 0.4
Belgium	8.53 ± 0.02	0.55 ± 0.02	34.8 ± 0.7	38.2 ± 0.7	41.6 ± 0.6	43.9 ± 1.2	38.6 ± 0.5
Croatia	6.268 ± 0.007	0.71 ± 0.02	30.9 ± 0.6	33.6 ± 0.7	36.6 ± 0.7	39.9 ± 1.1	30.9 ± 0.7
Denmark	7.667 ± 0.008	0.40 ± 0.01	35.6 ± 0.6	39.3 ± 0.5	42.8 ± 0.5	44.7 ± 1.2	39.4 ± 0.6
Finland	7.190 ± 0.005	0.385 ± 0.006	35.5 ± 0.7	39.2 ± 0.5	42.7 ± 0.5	44.5 ± 1.2	39.1 ± 0.6
France	7.711 ± 0.006	0.58 ± 0.012	36.2 ± 0.6	39.5 ± 0.6	42.9 ± 0.5	45.2 ± 1.2	39.9 ± 0.5
Germany	7.679 ± 0.007	0.62 ± 0.02	35.9 ± 0.6	39.2 ± 0.5	42.5 ± 0.4	45.1 ± 1.2	39.8 ± 0.5
Greece	5.537 ± 0.009	0.57 ± 0.02	32.5 ± 0.6	35.8 ± 0.5	39.2 ± 0.5	41.8 ± 1.2	32.6 ± 0.7
Hungary	6.022 ± 0.009	0.47 ± 0.01	34.0 ± 0.6	37.5 ± 0.5	41.0 ± 0.5	43.1 ± 1.1	37.6 ± 0.6
Ireland	8.580 ± 0.008	0.60 ± 0.02	33.0 ± 0.6	36.0 ± 0.7	39.4 ± 0.6	42.4 ± 1.2	37.0 ± 0.5
Italy	8.304 ± 0.004	0.429 ± 0.008	39.3 ± 0.7	43.0 ± 0.5	46.4 ± 0.5	48.2 ± 1.1	42.8 ± 0.5
Netherlands	7.904 ± 0.005	0.525 ± 0.008	35.1 ± 0.7	38.6 ± 0.6	42.1 ± 0.5	44.5 ± 1.2	39.0 ± 0.5
Norway	7.356 ± 0.006	0.58 ± 0.02	32.7 ± 0.6	35.8 ± 0.7	39.2 ± 0.6	42.0 ± 1.1	36.7 ± 0.5
Poland	7.13 ± 0.03	0.182 ± 0.007	46.3 ± 0.6	49.9 ± 0.6	53.2 ± 0.6	54.5 ± 1.3	49.4 ± 0.8
Slovakia	5.67 ± 0.02	0.59 ± 0.04	31.7 ± 0.7	34.8 ± 0.7	38.2 ± 0.6	40.9 ± 1.1	31.7 ± 0.7
Spain	8.747 ± 0.008	0.46 ± 0.01	38.2 ± 0.7	41.9 ± 0.5	45.3 ± 0.5	38.7 ± 1.1	38.5 ± 0.9
Switzerland	8.196 ± 0.003	0.72 ± 0.01	32.3 ± 0.6	35.0 ± 0.7	38.1 ± 0.7	41.5 ± 1.1	32.3 ± 0.6
UK	8.353 ± 0.007	0.368 ± 0.007	41.2 ± 0.7	44.9 ± 0.5	48.2 ± 0.6	49.8 ± 1.2	44.6 ± 0.6

TABLE I. Left block: parameters fitted from the first wave. Right block: median peak time of the second wave for the 5 typologies (cases a-e) we use in the simulations, with 1 standard deviation. The median and error only take into account the 100 simulations, differing by randomly generated matrices k_{ij} .

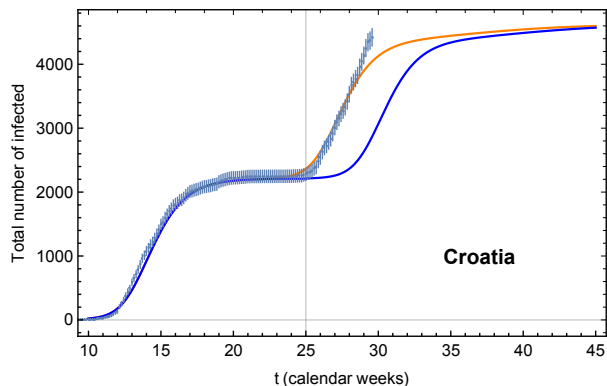


FIG. 2. Croatian number of total infected cases (not normalised per million) with respect to two theoretical curves. The blue one is the result of the simulation as described in the text. The orange curve is constructed by artificially shifting the second wave by three weeks, in order to match the timing in the data.

wave dynamics. For Croatia we also observe, however, that the total number of infected cases for the second wave is higher than for the first wave. It would be interesting to learn, from future data, whether this worrisome trend is followed by other European countries. The figure demonstrates that the result of our simple simulation can be tuned to reproduce the beginning of the second wave already observed in some countries. This fine tuning is,

however, beyond the scope of this work.

As an example of our results for other countries, we show in Fig. 3 the epidemic dynamics of the first and second wave for three representatives: Italy, France and the UK. The top panel shows the number of infected cases (solid lines) not normalised per million as well as the number of recovered cases (dashed curves). The central panel shows the number of new infected cases while the lower panel displays an estimate for the effective reproduction rate R . We also show the results for some of the Nordic countries, i.e. Denmark, Norway and Finland, in Fig. 4. The number of recovered cases $\mathcal{R}(t)$ is calculated by solving the following SIR-inspired equation [2]:

$$\frac{d\mathcal{R}}{dt} = \epsilon \left(e^{\alpha(t)} - \mathcal{R}(t) \right), \quad (3)$$

where we fix the recovery rate $\epsilon = 0.1$ in the numerical solutions. The effective reproduction rate R is estimated by computing the ratio of the new infected cases over the new recoveries within the susceptible population, from the theoretical model. The susceptible population is here defined as the total number of people infected at late time for the first and second waves independently. A more accurate result could be obtained using the generalised eRG approach of Ref. [3], at the expense of introducing more parameters. The plots are obtained using the simulations for case e). The height of the second wave peaks are the same as for the first wave because we used the same γ 's and a 's stemming from the first wave fit. One could allow for variations of these values, however the qualitative temporal picture of our results would remain similar.

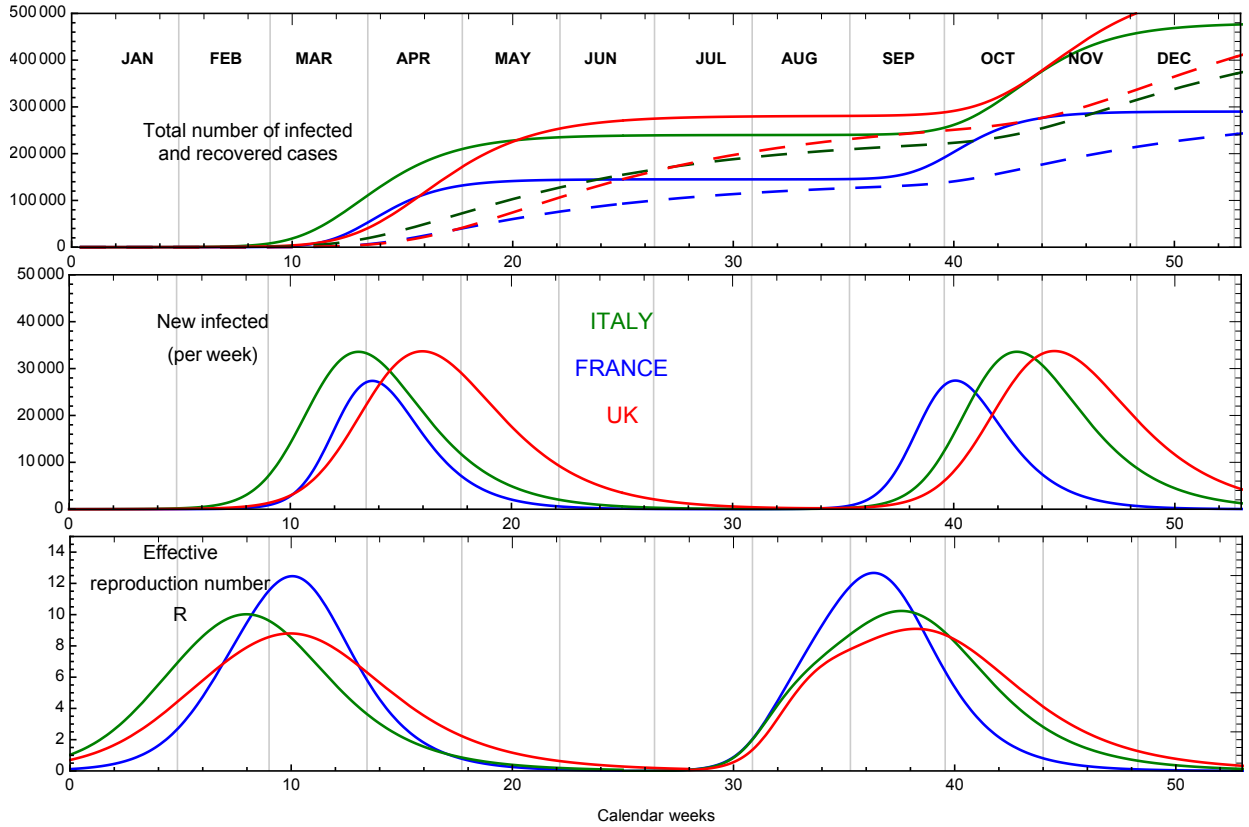


FIG. 3. Result of case e) for France, Italy and the UK. We show the time evolution of the total number of infected (solid) and recovered (dashed) cases in the top panel, the new infected in the central panel and the derived reproduction rate R_0 in the bottom panel. The number of cases refer to the total population of the countries. The shown solutions have a peak position close to the average value from the 100 simulations.

To study the dependence of the peak timing on k_{ij} , γ_i and a_i , we can use the results from cases a), b) and c) from Table I, as visualised in Fig. 5. Here we show the average peak time in calendar weeks versus γ for all the countries in this study. Comparing the results in each set of simulations, we discover a clear correlation between the timing of the peak and the infection rate γ_i of each country. The higher is the infection rate the sooner the peak is reached. Furthermore, comparing the results for the three cases, we show that reducing the coupling with Region-X systematically delays the peaks, in accordance with results reported in [2]. Quantitatively a reduction of a factor ten in the coupling to Region-X delays the peaks by about three weeks. We recall that, following the possible interpretations of Region-X, a reduction of the couplings to this region can be seen as the effect of travel bans and/or better control of local hotspots. Overall the peak timing ranges from end of July 2020 to beginning 2021. We did not find any correlation between the peak timing and the value of a_i across the countries we studied.

The results of cases d) and e), where only a few coun-

tries act as hotspots, as summarised in Table I, show a common feature: the peak timing of the hotspot countries is essentially the same we found in the unrestricted case a), as stemming from the k_{0i} values, while the peak timing for the other countries is substantially delayed. The fewer hotspots, 1 as in case d), the more delayed the peak. The results for case e), are shown in Fig. 6, with the hotspot countries highlighted in red. It should be clear that the a 's and the γ 's chosen for the simulation can, and will, be different from the first wave values we used. Nevertheless, we expect the dynamics to be still well represented by the framework and that these values give a reasonable indication for the second wave European pandemic.

III. DISCUSSION AND VIDEO SIMULATION

We employed the epidemic Renormalisation Group approach to simulate the dynamics of disease transmission and spreading across different European countries for the second COVID-19 wave. Since it has been demonstrated

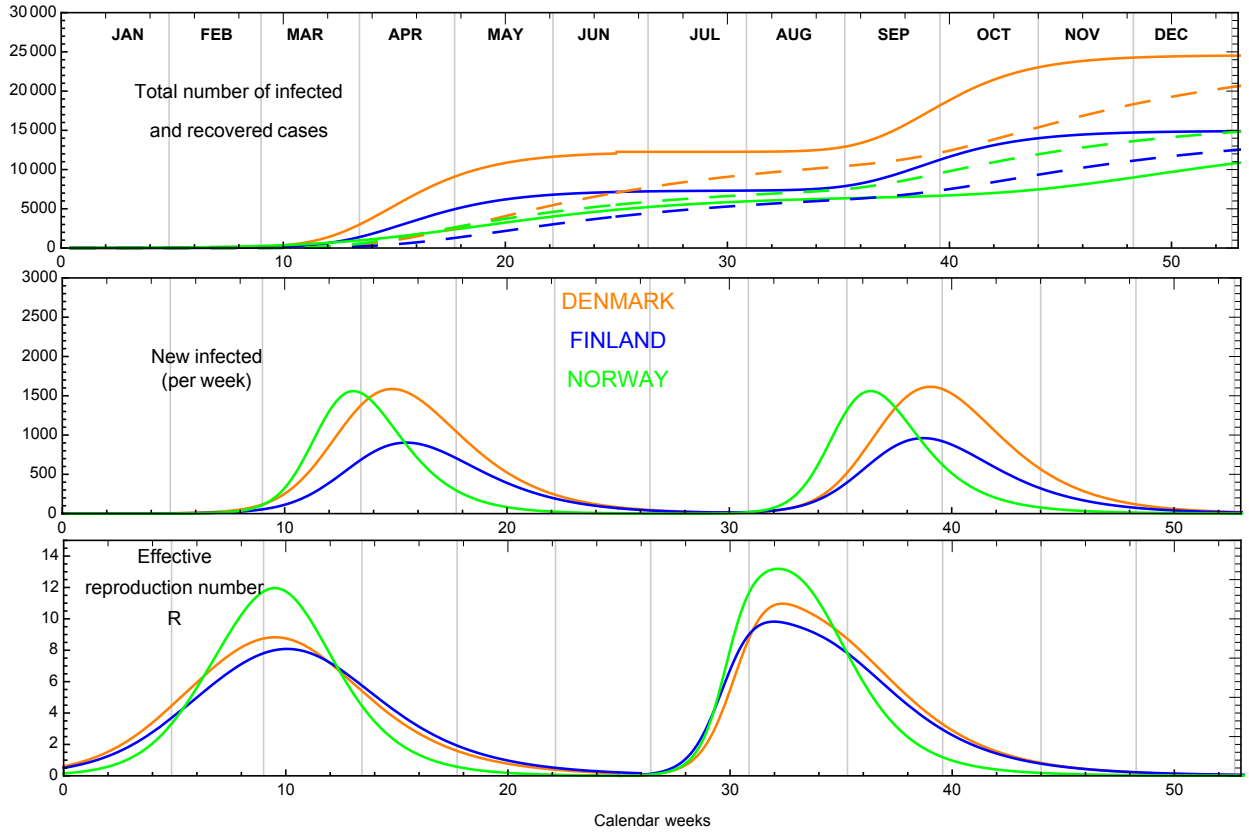


FIG. 4. Same as Fig. 3 for Denmark, Finland and Norway.

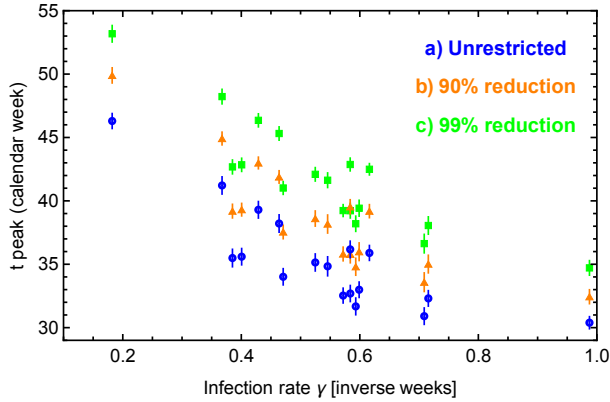


FIG. 5. Peak time, in calendar weeks, versus the infection rate γ for cases a), b) and c).

[3] that the framework can be mapped into other compartmental models, our results are sufficiently general. The approach allows to model inter and extra European border control effects while taking into account the impact of social distancing for each country. To reduce the number of unknowns in the simulation, we used the infor-

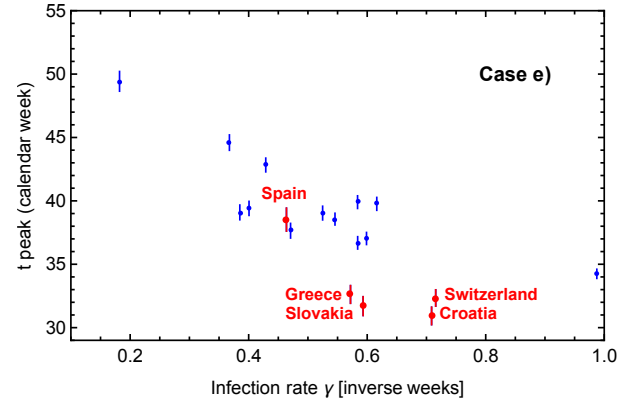


FIG. 6. Peak time, in calendar weeks, versus the infection rate γ for the case e) simulations, with the countries coupled to Region-X highlighted in red. The errors are one standard deviation on the statistics given by the 100 repetitions, as described in the text.

mation from the first wave. This information is encoded in the infection rate and the logarithm of the number of total infected cases per each country. Going beyond

this hypothesis is straightforward in our approach, but such parameter tuning is not the point of this work. We then performed statistical analyses averaging on different level of cross Europe interactions and with the rest of the world. The role of the rest of the world and possibly local hotspots has been attributed to a Region-X, which acts as a source of infection coupled to all or only few European countries. By calibrating on the current European situation that shows early signs of the second wave, we provided a temporal playbook of the second wave pandemic. Our results can be employed by governments, financial markets and the industry world to implement local and global measures.

The main results show that the temporal position of the second wave peak, once started, is rather solid and

will occur between July 2020 and January 2021. The precise timing for each country can be controlled via travel and social distancing measures.

In the added material, we also include an animation representing the time evolution of the first and second wave of the European COVID-19 pandemic resulting from one of our simulations close to the average result over 100 simulations for the most realistic case. The simplicity of the eRG approach is such that the simulations take only a few seconds on an average personal laptop, thus providing a practical and accurate tool for the understanding of a second (and third, and so on) wave pandemic. The temporal playbook we provide is a useful tool for governments, financial markets, the industries and individual citizens to prepare in advance and possibly counter the threat of recurring pandemic waves.

-
- [1] M. Della Morte, D. Orlando and F. Sannino, “Renormalization Group Approach to Pandemics: The COVID-19 Case,” *Front. in Phys.* **8** (2020), 144
Online here.
 - [2] G. Cacciapaglia and F. Sannino, “Interplay of social distancing and border restrictions for pandemics (COVID-19) via the epidemic Renormalisation Group framework,” [arXiv:2005.04956 [physics.soc-ph]].
 - [3] M. Della Morte and F. Sannino, “Renormalisation Group approach to pandemics as a time-dependent SIR model,” [arXiv:2007.11296 [physics.soc-ph]].
 - [4] W.O. Kermack and A.G. McKendrick, “A contribution to the mathematical theory of epidemics”, *Proceedings of the Royal Society A.* **115** (772): 700-721.
 - [5] K. G. Wilson, “Renormalization group and critical phenomena. 1. Renormalization group and the Kadanoff scaling picture,” *Phys. Rev. B* **4**, 3174 (1971).
 - [6] K. G. Wilson, “Renormalization group and critical phenomena. 2. Phase space cell analysis of critical behavior,” *Phys. Rev. B* **4**, 3184 (1971).
 - [7] L. Li, J. Zhang, C. Liu, H.T. Zhang, Y. Wang and Z. Wang, “Analysis of transmission dynamics for Zika virus on networks”, *Applied Mathematics and Computation*, **347**, 566 - 577. 2019.
 - [8] X.X. Zhan, C. Liu, G. Zhou, Z.K. Zhang, G.Q. Sun, J.J.H. Zhu and Z. Jin, “Coupling dynamics of epidemic spreading and information diffusion on complex networks”, *Applied Mathematics and Computation*, **332**, 437 - 448, 2018.
 - [9] M. Perc, J.J. Jordan, D.G. Rand, Z. Wang, S. Boccaletti and A. Szolnoki, “Statistical physics of human cooperation”, *Physics Reports* **687**, 1-51, 2017.
 - [10] Z. Wang, M.A. Andrews, Z.X. Wu, L. Wang and C.T. Bauch, “Coupled disease-behavior dynamics on complex networks: A review”, *Physics of Life Reviews*, **15**, 1 - 29, 2015.
 - [11] Z. Wang, C.T. Bauch, S. Bhattacharyya, A. d’Onofrio, P. Manfredi, M. Perc, N. Perra, M. Salathe and D.W. Zhao, “Statistical physics of vaccination”, *Physics Reports*, **664**, 1 - 113, 2016.
 - [12] J.M.A. Danby, “Computing applications to differential equations modelling in the physical and social sciences”, Reston, Va.: Reston Publishing Company, 1985.
 - [13] F. Brauer, “Early estimates of epidemic final sizes”, *Journal of Biological Dynamics* **13** (sup1):23-30. 2019.
 - [14] J.C. Miller, “A note on the derivation of epidemic final sizes”, *Bulletin of mathematical biology* **74** (9):2125-2141. 2012
 - [15] J.D. Murray, “Mathematical biology”, 3rd ed, Interdisciplinary applied mathematics. New York: Springer. 2002.
 - [16] D. Fisman, E. Khoo and A. Tuite, “Early Epidemic Dynamics of the West African 2014 Ebola Outbreak: Estimates Derived with a Simple Two-Parameter Model”, *PLOS Currents Outbreaks*, 2014 .
 - [17] B. Pell, K. Yang, C. Viboud and G. Chowell, “Using phenomenological models for forecasting the 2015 Ebola challenge”, *Epidemics* **22**:62-70, 2018.
 - [18] D.Faranda and T.Alberti, “Modelling the second wave of COVID-19 infections in France and Italy via a Stochastic SEIR model”, arXiv:2006.05081 (2020).

AUTHOR CONTRIBUTION

This work has been designed and performed jointly and equally by the authors. G.C., C.C. and F.S. have equally contributed to the writing of the article.

COMPETING INTERESTS

The authors declare no competing interests.